Scilight

Energy Safety Science and Technology
https://www.sciltp.com/journals/esst

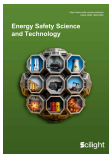

Article

Hazard Suppression Effect of Liquid Thermal Management System on External Short Circuit of Large-Capacity $LiFePO_4$

Chun E [1], Xiaoming Jin [1], Hui Zhang [2], Jialei Liu [2] and Jialong Liu [1,*]

[1] College of Safety Science and Engineering, Nanjing Tech University, Nanjing 21009, China
[2] College of Chemical Engineering, Nanjing Tech University, Nanjing 21009, China
* Correspondence: jialliu@njtech.edu.cn

How To Cite: E, C.; Jin, X.; Zhang, H.; et al. Hazard Suppression Effect of Liquid Thermal Management System on External Short Circuit of Large-Capacity $LiFePO_4$. *Energy Safety Science and Technology* **2026**, *1*(1), 4.

Received: 26 May 2026
Revised: 24 June 2026
Accepted: 8 July 2026
Published: 24 July 2026

Abstract: To investigate the thermal behavior and capacity degradation of lithium-ion batteries under external short-circuit conditions with liquid cooling thermal management, this study used 50 Ah prismatic lithium iron phosphate batteries as the research objects. An external short-circuit test platform and a liquid cooling system were established to analyze the variations in voltage, current, temperature, and depth of discharge. The effects of coolant temperature and flow rate on the battery thermal response were further examined. Combined with heat transfer calculation, capacity testing, incremental capacity analysis, and impedance analysis, the aging mechanism after external short circuit were investigated. The results show that the external short-circuit process can be divided into five stages: rest, short-circuit initiation, current plateau, over-discharge heating, and cooling stabilization. During the early stage, the voltage drops rapidly, the current rises sharply, and Joule heat dominates heat generation. As discharge continues, temperature rise affects internal impedance and current evolution. In the over-discharge stage, side-reaction heat contributes more to temperature rise. Liquid cooling suppresses both the temperature rise rate and maximum temperature, while reducing side-reaction heat generation. Without liquid cooling, the capacity loss reaches 5.79%, whereas liquid cooling reduces it to 1.45–2.35%. Lower coolant temperature and higher flow rate help mitigate capacity degradation, with coolant temperature showing a stronger influence. Incremental capacity and impedance analyses indicate that external short circuit causes active lithium loss, electrode structural damage, and impedance increase, while liquid cooling can alleviate these aging effects. This study provides guidance for battery safety protection, liquid cooling optimization, and post-fault health evaluation.

Keywords: lithium iron phosphate battery; external short circuit; liquid cooling thermal management

1. Introduction

With the rapid development of new energy vehicles and energy storage systems, lithium-ion batteries have been widely used in power battery systems and electrochemical energy storage systems due to their high energy density, long cycle life, and high charge-discharge efficiency. However, batteries do not always operate under ideal conditions in practical applications. Their safety and service life are affected by various factors, such as temperature, charge-discharge rate, state of charge, and external electrical faults. Previous studies have shown that battery temperature is a key parameter affecting the performance, lifetime, and safety of lithium-ion batteries.

Excessively high temperature may induce thermal runaway, combustion, or even explosion, while excessively low temperature can also lead to capacity decline and operational failure [1–6]. Therefore, during battery operation, controlling battery temperature rise, improving temperature uniformity, and reducing safety risks under abnormal conditions through effective thermal management have become important issues in power battery safety research.

External short circuit is one of the typical electrical abuse in lithium-ion batteries. When a low-resistance connection is formed externally between the positive and negative terminals of a battery, the battery releases a large amount of electrical energy within a short period, resulting in a rapid voltage drop, a sharp increase in discharging current, and a rapid temperature rise [7,8]. Chen et al. [9] investigated the temperature rise of lithium-ion batteries during ESC and found that the maximum temperature rise was strongly affected by the state of charge and ambient temperature. Zhao et al. [10] studied the electrical and thermal responses of batteries during ESC and found that battery capacity and structural parameters significantly affected their thermal behavior. Liu et al. [11] investigated the effects of multiple factors on ESC and found that the electrical and thermal responses were jointly influenced by operating conditions and battery characteristics. Yu et al. [12] studied thermal-runaway-induced short-circuit arcs in highly integrated battery systems and found that the case-to-case arc was the most hazardous mode, with temperatures exceeding 1400 °C under critical voltage and electrode-spacing conditions. These studies demonstrate that ESC is a complex electro-thermal coupling process involving current, internal resistance, polarization, heat generation, and heat dissipation.

Under external short-circuit, the thermal behavior of batteries is influenced by the initial state of charge, short-circuit resistance, short-circuit current, ambient temperature, and battery structure. An et al. [13]. investigated the electro-thermal behavior of $LiFePO_4$ batteries during external short circuit and found that the battery temperature rise and temperature rise rate were closely related to the short-circuit current and initial state of charge. In addition, electrode degradation phenomena such as electrolyte consumption, metal deposition, particle cracking, separator pore closure, and increased internal resistance may occur after external short circuit. Yang et al. [14] studied external short-circuit faults in electric vehicle battery packs and further demonstrated that single battery and battery packs exhibit different responses under external short-circuit conditions. Therefore, the identification and prediction of external short-circuit faults should be combined with the actual operating characteristics of battery packs. Hence, when studying external short-circuit safety, analyzing only the temperature rise behavior of a single battery under natural heat dissipation is insufficient to fully reflect the thermal response characteristics of real power battery systems.

Liquid cooling thermal management is one of the most widely used thermal management methods in current power battery systems [15,16]. Compared with air cooling, liquid cooling systems have stronger heat transfer capability, more flexible structural arrangement, and better suitability for high-power-density battery packs. Wu et al. [17] reviewed liquid-cooling plate systems and identified the maximum temperature, maximum temperature difference, and pressure drop as key indicators for evaluating cooling performance. Lai et al. [18] designed a compact liquid-cooling system for cylindrical battery packs and found that the cooling structure and coolant flow rate significantly affected battery temperature and temperature uniformity. Li et al. [19] developed liquid cold plates with pin-fin microchannels and found that the pin fins effectively reduced both the maximum temperature rise and temperature difference of the battery. Wang et al. [20] investigated topology-optimized cold plates under laminar and turbulent flow conditions and found that topology optimization could improve temperature uniformity while balancing heat-transfer performance and pressure drop. However, under abnormal high-heat-generation conditions such as external short circuit, the role of a liquid cooling system is not limited to reducing the battery surface temperature. It may also alter the heat release path, local hot spot distribution, and high-temperature duration, thereby influencing the battery thermal safety boundary and post-fault performance degradation.

In addition to instantaneous thermal safety risks, external short circuit may also have a continuous impact on subsequent battery capacity and service life. Battery capacity degradation is generally associated with loss of active lithium, loss of active materials, increased impedance, and SEI film growth [13,14]. During external short circuit, high-current impact and rapid temperature rise can intensify electrode polarization and side reactions, potentially causing electrode structural damage, separator thermal shrinkage, electrolyte decomposition, and uneven interfacial film growth. Zhang et al. [21] investigated the effect of short-time external short circuit on the long-term cycling capacity fading mechanism of $LiCoO_2$/MCMB batteries and found that external short circuit affects subsequent polarization behavior and capacity retention. Furthermore, An et al. [22] showed that external short-circuit duration is highly correlated with battery temperature rise and capacity degradation, and longer short-circuit duration leads to more pronounced temperature rise, capacity loss, and internal resistance increase. This indicates that even if thermal runaway does not occur immediately during external short circuit, the internal structure and electrochemical performance of the battery may already have suffered irreversible damage.

To address the above research gap, this study investigates the hazard-suppression effect of liquid cooling thermal management on the external short circuit of a 50 Ah prismatic $LiFePO_4$ battery. First, the variations in voltage, current, temperature, and depth of discharge during external short circuit are analyzed, and the process is divided into characteristic stages according to the evolution of these parameters. Second, the effects of coolant temperature and flow rate on the battery electro-thermal response are examined to evaluate the ability of liquid cooling to suppress temperature rise and heat accumulation. Third, an energy-balance analysis is conducted to quantify the contributions of Joule heat, side-reaction heat, and heat dissipation during the short-circuit process. Finally, capacity testing, incremental capacity analysis, and impedance analysis are employed to reveal the post-fault degradation behavior and clarify the relationship among thermal history, side reactions, electrode damage, capacity loss, and impedance growth. The results provide a theoretical and experimental basis for external-short-circuit protection, liquid-cooling parameter optimization, and post-fault health assessment of power batteries.

2. Experimental Setup

2.1. Experimental Materials

In this experiment, a 50 Ah prismatic lithium iron phosphate battery was used as the research object. The physical image of the battery is shown in Figure 1, and its characteristic parameters are listed in Table 1.

Figure 1. Physical image of 50 Ah lithium iron phosphate prismatic battery.

Table 1. Characteristic parameters of 50 Ah lithium iron phosphate prismatic battery.

Name	Parameter
Positive/Negative	$LiFePO_4$/Graphite
Size (length × width × height)	(148.2 × 27 × 134.7) mm
Nominal capacity	50 Ah
Standard charge/discharge rate	0.5 C (25 A)
Nominal voltage	3.2 V
Charging/Discharging cut-off voltage	3.65 V/2 V
Specific heat capacity	1029.49 J/(kg·°C)

2.2. Treatment of Lithium-Ion Batteries before and after Experiments

Before the external short-circuit test, the 50 Ah lithium iron phosphate battery was cycled three times for capacity activation. The specific procedure was as follows: constant current-constant voltage (CC-CV) charging, the battery was charged to 3.65 V at a current rate of 0.5 C. After resting until the battery voltage became stable, the battery was discharged to 2 V at 0.5 C under constant-current (CC) mode. After three cycles, the discharge capacity of the last cycle was taken as the actual battery capacity, and the battery was then charged to 100% SOC under CC-CV mode. After the three cycles and full charging to 100% SOC, the initial capacity and IC curve of the battery were obtained. In addition, an HPPC test was conducted to determine the internal resistance of the battery.

After the external short-circuit test, the 50 Ah lithium iron phosphate battery was charged to 3.65 V at 0.5 C under CC-CV mode. After resting until the battery voltage became stable, the battery was discharged to 2 V at 0.5 C under CC

mode. The capacity and IC curve of the battery after the external short-circuit test were then obtained. Meanwhile, an HPPC test was performed to determine the internal resistance of the battery after the external short circuit.

2.3. External Short-Circuit Test and External Short Circuit Under Thermal Management System Test

The experiment was conducted in a combustion chamber with dimensions of 210 cm × 190 cm × 190 cm. The experimental setup includes thermostatic water bath, peristaltic pump, battery test system, temperature collector, camera, computer, relay model, hall current sensor and paperless recorder. It is shown in Figure 2. The experiments include external short circuit test and external short circuit under thermal management system test. During external short circuit test, the lithium-ion battery is fixed on the experimental table by stainless steel fixtures. Mica plate was placed between the fixtures and battery to avoided heat transfer between them. K-type thermocouple was attached to the surface of lithium-ion battery to detect temperature change of battery. Battery test system was used to detect voltage change of battery. Hall current sensor and paperless recorder were used to detect and record discharging current during external short circuit. Relay model was used to open and close the external circuit.

The external short circuit under thermal management system test is similar to the external short circuit test. The difference is that the liquid cooling plate is attached to the large surface of battery closely. The mica plate was also placed between the fixture and liquid cooling plate to avoid heat transfer between them. The temperature, discharging current and voltage were obtained to compare them to the results in external short circuit test. To find the influence of liquid cooling parameter on the external short circuit behavior, the flow rate and coolant temperature were selected as different values (1.5 L/min, 1 L/min, 0.5 L/min; 5 ℃, 10 ℃, 15 ℃).

After external short circuit and external short circuit under thermal management system tests, capacity and HPPC tests were conducted to obtain capacity and resistances of batteries. The results were compared to their initial capacity and resistance before tests. Afterwards, the hazard suppression function of liquid thermal management system in external short circuit can be found.

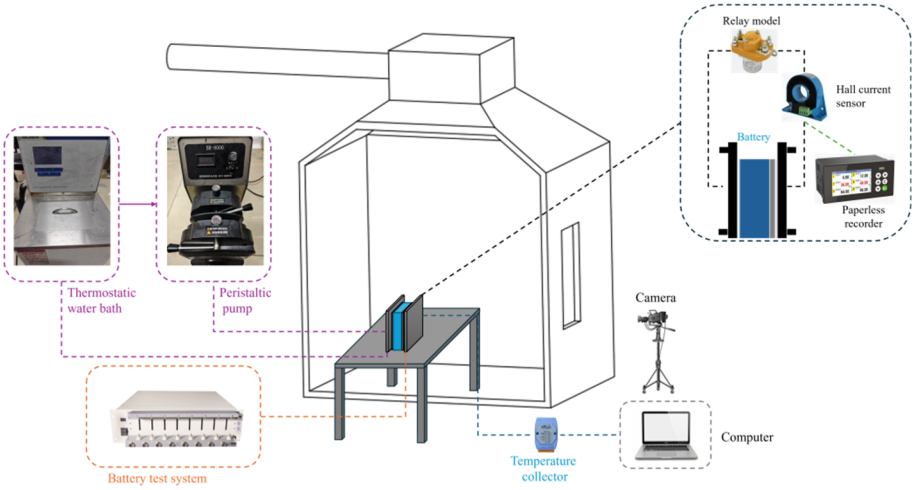

Figure 2. Schematic diagram of external short circuit experiment setup.

3. Results and Discussion

3.1. Characteristics of the External Short-Circuit Behavior in Lithium Iron Phosphate Batteries

The variations in battery temperature, voltage, current, and depth of discharge during external short circuit are shown in Figure 3. Based on the changes in the characteristic parameters of the battery, the external short circuit process of battery can be divided into five stages.

In the first stage, the battery was in a resting state. At this time, the battery temperature and voltage remained unchanged, and the battery was at 100% SOC, corresponding to 0% DOD. The external short circuit had not yet started, and the current was 0 A. The battery impedance consisted of lithium diffusion resistance in solid particles (R_s), lithium migration resistance in the electrolyte (R_l), charge transfer resistance caused by electrochemical reactions on the surface of electrode active materials (R_{ct}), and electronic conduction resistance (R_e). As shown in Equation (1), the terminal voltage of the battery is the sum of the open-circuit voltage and the overpotential, which is negative during discharge. When the current is 0, the terminal voltage of the battery is equal to the open-circuit voltage.

$$V_t = \mathrm{OCV} + IR = \mathrm{OCV} + I(R_s + R_{ct} + R_l + R_e) \quad (1)$$

In the second stage, the external short circuit of battery is triggered by closing the external circuit. The battery voltage rapidly decreased to approximately 2.55 V, while the discharge current increased to 241.94 A, and the battery surface temperature began to rise. Subsequently, the voltage increased slowly, and the current decreased to a local minimum of 179.49 A. After the external circuit was closed by the relay model, electrons moved rapidly through the external circuit wires. Under the high potential difference between the positive and negative electrodes, electrochemical reactions occurred rapidly on the surfaces of the positive and negative active materials.

At the moment of external circuit closing, the battery current increased rapidly owing to low ohmic resistance and charge transfer resistance and high open circuit voltage. Due to the sensitivity of the Hall current sensor and paperless recorder, one discharging current data was recorded per second. Subsequently, lithium on the surfaces of the negative and positive active materials was rapidly consumed and accumulated, respectively, forming concentration gradients inside the active material particles. This caused high diffusion resistance in solid particles. Meanwhile, lithium ions in the electrolyte near the surfaces of the negative and positive active materials rapidly increased and decreased. Assuming that the lithium ion concentration in the electrolyte far from the active material surface remained constant, a concentration gradient existed between the electrolyte near the electrode surfaces and that far from the active materials, resulting in a continuous increase in the lithium-ion migration resistance in the electrolyte.

Since the positive and negative active materials of lithium-ion batteries are porous electrodes, the local increase and decrease in lithium ion concentration in the electrolyte near the negative and positive electrodes were further intensified. Due to the increase and decrease of lithium ions, the electrochemical reactions on the surfaces of the negative and positive electrodes were suppressed, leading to an increase in charge transfer resistance. According to the study of Liu et al. [23], the ohmic resistance of lithium-ion batteries does not change with SOC. As shown in Equation (1), the decrease in OCV and the increase in impedance during external short circuit caused the decrease in battery current. In this stage, the increase in polarization resistance was the main reason for the decrease in battery current. According to Joule's law, the high discharge current caused the battery surface temperature to rise. In this stage, the maximum temperature of battery was 13.4 °C, which was lower than the onset temperature of exothermic side reactions. However, the rapid extraction and insertion of lithium ions in the negative and positive electrode materials could damage the SEI and CEI films, thereby inducing weak side reactions. As shown in Figure 3, the temperature rise rate of the battery changed slightly, and Joule heat remained the main heat generation source in this stage.

In the third stage, as shown in Figure 3, the discharge current slowly increased after decreasing to the minimum value in the second stage. At the end of this stage, the discharge current decreased rapidly, while the battery temperature continued to increase. This indicates that the lithium ion concentration gradients in the positive and negative active material particles, as well as the concentration gradients in electrolyte, tended to become stable in this stage. The electrochemical reactions also became relatively stable. The lithium-ion diffusion resistance in solid particles, the migration resistance in the electrolyte, and the charge transfer resistance tended to stabilize.

However, the battery temperature continued to rise. At high temperature, the diffusion rate of lithium ions in solids and the migration rate in the electrolyte increased, and the electrochemical reaction rate was also accelerated, thereby reducing the battery impedance and causing the slowly increase in discharge current. At the end of this stage, the DOD reached 100%. In the later period of discharge, the battery capacity was gradually depleted. The negative active material tended to become fully delithiated, while the positive electrode tended to become fully lithiated. Lithium ions became more difficult to extract from and insert into the negative and positive electrodes. This caused the rapid increase in lithium diffusion resistance in solid particles and the charge transfer resistance. Meanwhile, the battery OCV continuously decreased, leading to a rapid decrease in both battery current and terminal voltage. The decrease in battery current means less Joule heat generation, and the temperature rise rate of the battery decreased.

In the fourth stage, over-discharge occurred. The voltage and current rapidly decreased. The battery temperature rise rate decreased sharply, and the temperature slowly increased to 63.2 °C. After the battery was fully discharged, lithium ions in the negative electrode were completely extracted and inserted into the positive electrode, causing rapid decrease of OCV. As over-discharge proceeded, the SEI film on the negative electrode decomposed, resulting in a significant increase in the internal impedance of the battery. The battery exhibited strong polarization, the terminal voltage decreased, and the current rapidly declined, leading to a reduction in Joule heat generation. Gotz et al. [24] reported that when the battery temperature exceeds 60 °C, part of the SEI inside the battery begins to decompose. In addition, side reactions caused by battery over-discharge also generated a certain amount of heat. In this stage, the main heat generation source was side-reaction heat.

In the fifth stage, the battery voltage and current gradually decreased to 0 V and 0 A, and the battery temperature began to decrease. The potential difference between the positive and negative electrodes gradually narrowed until the potentials of the positive and negative electrodes eventually became equal, and the terminal voltage of the battery reached 0 V. The internal side reactions of the battery tended to stabilize. The heat generated by internal side reactions continuously decreased and gradually became lower than the heat dissipated by the battery, resulting in a decrease in battery temperature.

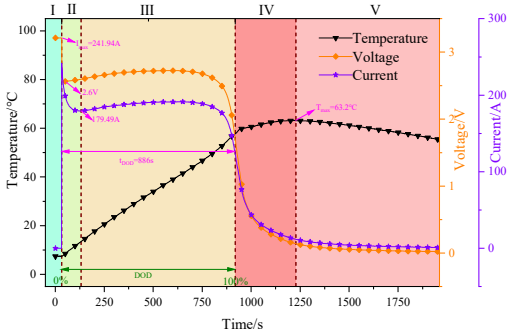

Figure 3. Thermal characteristics of external short circuit in lithium iron phosphate batteries.

3.2. Influence of Different Liquid Cooling Thermal Management Parameters on the External Short-Circuit Behavior of the Battery

As described above, external short circuit of the battery induces polarization and heat accumulation. To reduce the influence of high temperature on battery performance, a liquid cooling thermal management system was used in this study to dissipate heat from the battery. The effects of different liquid cooling parameters on external short-circuit behavior were analyzed. Distilled water was used as the coolant in the liquid cooling thermal management system. By changing the flow rate and temperature of the coolant, the effects of two parameters on battery external short-circuit behavior were investigated. The variations in temperature, voltage, current, and depth of discharge of the lithium-ion battery under the liquid cooling thermal management system during external short circuit are shown in Figure 4. Based on the changes in the characteristic parameters of the battery, the external short-circuit process can also be divided into five stages. In the first stage, similar to the experiment in Section 3.1, the battery was in a resting state. The battery temperature and voltage remained unchanged, the battery was at 0% DOD, and the external short circuit had not yet started. The current was 0 A.

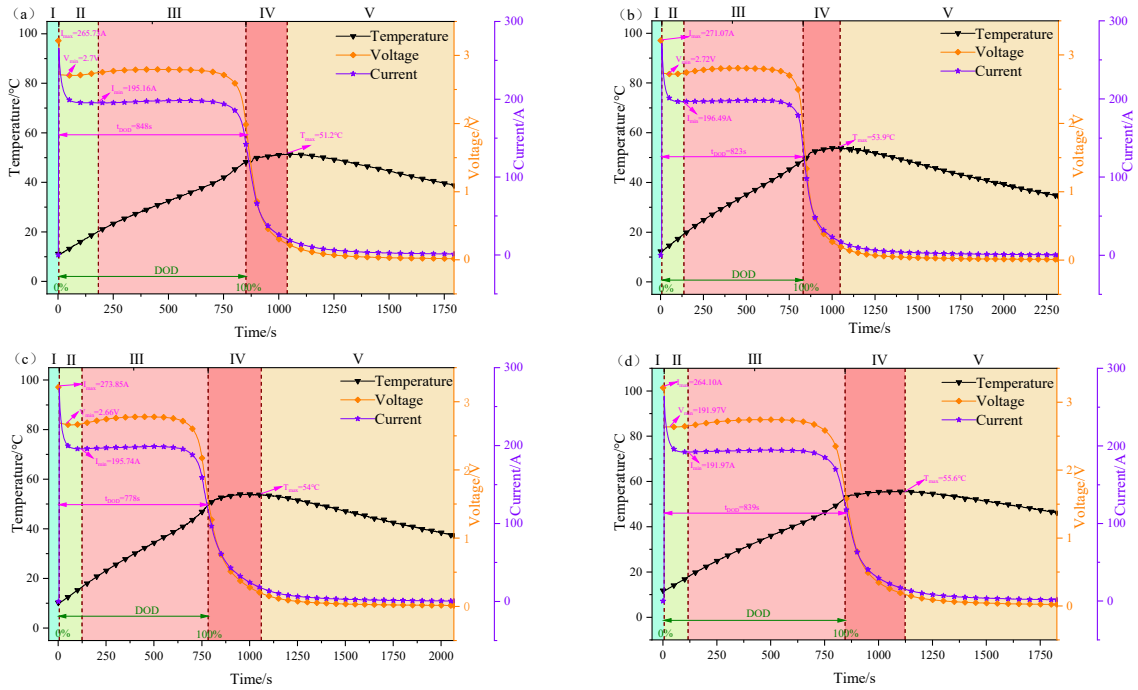

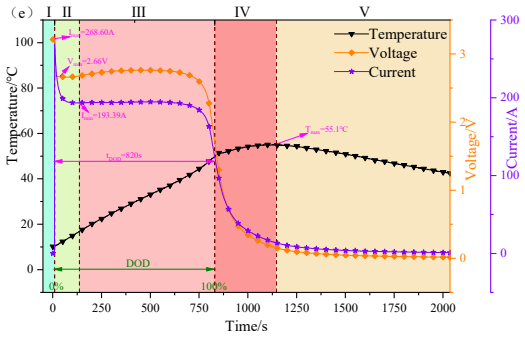

Figure 4. External short-circuit behavior of the battery under different liquid-cooling parameters: (**a**) 5 °C-1.5 L/min; (**b**) 10 °C-1.5 L/min; (**c**) 15 °C-1.5 L/min; (**d**) 5 °C-1.0 L/min; (**e**) 5 °C-0.5 L/min.

In the second stage, the external short circuit was triggered. The battery voltage decreased rapidly, the discharge current increased instantly, and the battery surface temperature began to rise. Subsequently, the battery voltage increased slowly, while the current began to decrease and reached a local minimum value. This behavior was generally consistent with the external short-circuit characteristics described above. The initial temperature of the battery under the external short circuit was much lower than that in the other experiments, as the room temperature was relatively lower than the temperature of cooling plate. The increase in temperature promoted the charge transfer reaction and accelerated lithium migration, thereby reducing the battery impedance. The maximum current under the external short circuit was only 241.94 A, whereas the maximum external short-circuit current under liquid cooling conditions was higher. Moreover, as the coolant temperature increased, the maximum battery current increased. However, with the increase in coolant flow rate, the maximum external short-circuit current changed only slightly, because the initial battery temperatures were similar.

The duration of the second stage was prolonged under liquid cooling thermal management. As mentioned above, the increase in battery current was caused by the decrease in battery impedance resulting from the rise in battery temperature. Liquid cooling slowed down the increase in battery temperature, thereby slowing the decrease in battery impedance and delaying the rise in battery current. As the coolant flow rate decreased and the coolant temperature increased, the duration of this stage became longer. During this stage, Joule heat generated by the current was the main heat source, and a lower current resulted in less heat generation. Therefore, the battery temperature at the end of the second stage was the lowest in the external short circuit experiment.

In the third stage, the battery temperature continued to increase, and the discharge current of the battery increased slowly in all experiments. The increase in temperature promoted lithium diffusion in solid particles and migration in the electrolyte, and also enhanced the electrochemical reaction rate, thereby reducing the battery impedance. It is shown in Figure 5 that the increase in battery current was the most significant under the external short circuit test, whereas the current variation was not obvious in the experiments with liquid cooling. In the external short circuit experiment, the battery temperature increased significantly from 13.5 °C to 57.7 °C as shown in Table 2. The high temperature affected the lithium migration rate and electrochemical reaction rate inside the battery, reducing the impedance and causing a significant increase in the discharge current. Under liquid cooling thermal management, the battery temperature rise rate was suppressed, resulting in a slower increase in battery temperature. Therefore, its influence on lithium-ion migration and electrochemical reaction rates inside the battery was relatively small, and the variation in discharge current was also small.

Table 2. Variation of battery characteristic parameters in the third stage under different external short-circuit experiments.

The Third Stage	Starting Temperature (°C)	End Temperature (°C)	Average Current (A)	Discharge Time (s)
ESC	13.5	57.7	184.78	886
ESC-5 °C-1.5 L/min	20.3	48.2	194.61	848
ESC-10 °C-1.5 L/min	19.4	48.7	195.09	823
ESC-15 °C-1.5 L/min	16.6	49.6	192.71	778
ESC-5 °C-1 L/min	17.9	52.6	189.59	839
ESC-5 °C-0.5 L/min	16.8	49.8	190.07	820

As shown in Figure 4, when the coolant temperature increased, the discharge current in the third stage changed slightly. However, when the coolant flow rate decreased, the battery current was relatively lower. As shown in Table 2, at a constant coolant flow rate of 1.5 L/min, increasing the coolant temperature from 5 to 15 °C increased the temperature rise during the third stage, while the stage duration decreased. The average current varied

only slightly, ranging from 192.71 to 195.09 A. A higher coolant temperature reduced the temperature difference between the battery and the coolant, thereby weakening heat removal and increasing heat accumulation. The resulting temperature increase promoted lithium diffusion, migration, and charge-transfer reactions, causing the battery to reach the late-discharge stage earlier. Therefore, under a constant flow rate, coolant temperature mainly affected the battery temperature rise and the duration of the third stage, whereas its influence on the average current was relatively limited.

As shown in Table 2, at a constant coolant temperature of 5 °C, reducing the coolant flow rate from 1.5 to 1.0 L/min increased the temperature and reduced the average current. When the flow rate was further reduced to 0.5 L/min, the temperature rise was 33.0 °C, the average current was 190.07 A, and the third-stage duration decreased to 820 s. In general, reducing the coolant flow rate weakened the convective heat-transfer capacity and increased heat accumulation relative to the 1.5 L/min condition.

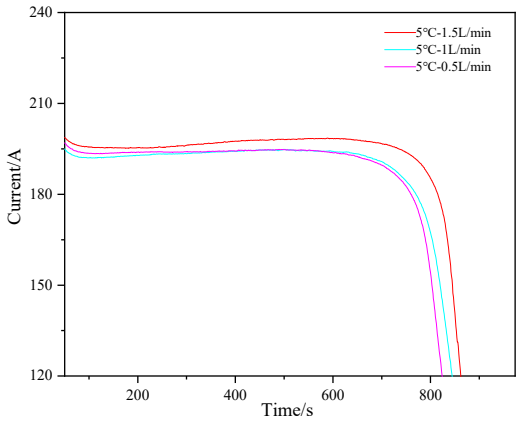

Figure 5. Variation of battery current in the third stage under different external short-circuit experiments.

In the fourth stage, the battery was over-discharged after being discharged to 100% DOD. The voltage and current decreased rapidly. During this stage, the changes in the battery were generally similar. The battery temperature was relatively low, the exothermic side reactions inside the battery were weak, and the heat generation was limited. Under the action of the liquid cooling thermal management system, the heat generated by internal side reactions in the battery was dissipated more quickly, ultimately causing the battery temperature to increase less, as shown in Table 3. In addition, when the liquid cooling temperature remained unchanged and the liquid cooling flow rate gradually decreased, the battery surface temperature increased. However, it can be found that in the experiments with flow rates of 1 L/min and 0.5 L/min, the maximum battery temperatures were almost the same. This indicates that when the coolant flow rate of the liquid cooling thermal management system decreases to a certain value, the change in the heat dissipation effect of liquid cooling thermal management on battery external short circuit becomes very small.

Table 3. Changes in battery characteristic parameters during the fourth stage across different external short-circuit experiments.

The Four Stage	Starting Temperature (℃)	End Temperature (℃)
ESC	57.7	63.2
ESC-5 °C-1.5 L/min	48.2	51.2
ESC-10 °C-1.5 L/min	48.7	53.9
ESC-15 °C-1.5 L/min	49.6	54
ESC-5 °C-1 L/min	52.6	55.6
ESC-5 °C-0.5 L/min	49.8	55.1

In the fifth stage, the internal side reactions of the battery tended to stabilize. The heat generated by the internal side reactions continuously decreased and gradually became lower than the heat dissipated by the battery. Under the action of liquid cooling, the battery temperature decreased rapidly.

3.3. Heat Generation Analysis of the Battery during External Short Circuit

During the external short-circuit process of the battery, the heat variation of the battery includes Joule heat caused by current Q_J, heat generated by internal side reactions Q_S, heat dissipated by liquid cooling Q_d and

convective and radiative heat transfer between the upper surface of the battery and the air Q_{conv} and Q_{rad}。 Therefore, the change in the internal energy of the battery can be obtained by Equation (2):

$$mc_p\Delta T = Q_J + Q_s + Q_{conv} + Q_{rad} + Q_d \quad (2)$$

Here, m represents the mass of the battery; c_p denotes its specific heat capacity; and ΔT indicates the temperature change of the battery.

According to Joule's law, the Joule heat generated in a battery can be calculated using Equation (3):

$$Q_J = \int_{t_1}^{t_2} q_J dt = \int_{t_1}^{t_2} I^2 R_{tot} dt = \int_{t_1}^{t_2} I^2 (R_\Omega + R_P) dt = \int_{t_1}^{t_2} UI dt \quad (3)$$

Here, q_J represents the joule heat generation rate.

According to Equation (1), R_{tot} can be obtained using Equation (4):

$$R_{tot} = \frac{V_t - OCV}{I} \quad (4)$$

The upper surface of the battery is in contact with the air, exchanging heat with it through thermal convection and radiation. This process can be calculated using Newton's law of cooling and Boltzmann's law, as shown in Equations (5)–(8):

$$q_{conv}(t) = h \times (T_{Up} - T_\infty) \quad (5)$$

$$q_{rad}(t) = \varepsilon \times \sigma \times ({T_{Up}}^4 - {T_\infty}^4) \quad (6)$$

$$Q_{conv} = A \int_{t_1}^{t_2} q_{conv}(t) dt \quad (7)$$

$$Q_{rad} = A \int_{t_1}^{t_2} q_{rad}(t) dt \quad (8)$$

Here, h is the convective heat transfer coefficient, equal to 5 W/(m^2·K) [25]; the emissivity ε is 0.15 [26]; the Boltzmann constant σ is 5.670373 × 10^{-8} W/(m^2·K^4); A is the surface area of the battery, measuring 0.003618 m^2; T_{up} is the temperature of the battery's upper surface; and T_∞ is the ambient temperature.

Based on the aforementioned methods, the contribution of different heat-generating processes to the total heat production can be calculated using Equation (9) (using joule heat as an example):

$$Q_J = \frac{\int_{t_1}^{t_2} I^2 R_{tot} dt}{Q_{tot}} \quad (9)$$

Among them, Q_{tot} represents the total heat generation.

Based on the above descriptions, Figure 6 illustrates the varying heat generation patterns of lithium-ion batteries during short circuits.

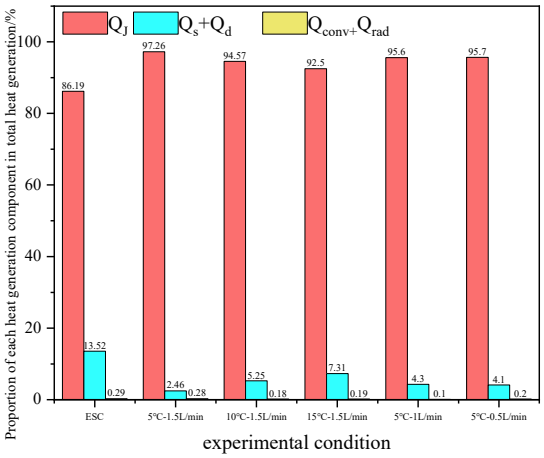

Figure 6. Proportion of each heat generation to total heat generation during battery external short circuit.

As shown in Figure 6, the heat generated during the external short-circuit process was mainly composed of Joule heat and heat generated by internal side reactions. Under the external short circuit test without liquid cooling, the rapid temperature rise and substantial heat accumulation resulted in greater side-reaction heat generation. After liquid cooling was used, the heat generated by internal side reactions was significantly reduced.

At a constant coolant flow rate of 1.5 L/min, the proportion of side-reaction heat gradually increased with increasing coolant temperature. This indicates that a higher coolant temperature weakened the heat-dissipation capacity of the liquid-cooling system and promoted temperature-sensitive side reactions. At a constant coolant temperature of 5 °C, the proportions of side-reaction heat at flow rates of 1.5, 1.0, and 0.5 L/min were 2.46%, 4.30% and 4.10%, respectively. Compared with the 1.5 L/min condition, reducing the coolant flow rate generally increased the contribution of side-reaction heat.

Overall, liquid cooling effectively slowed the battery temperature rise, reduced heat accumulation, and delayed or suppressed the occurrence of internal side reactions.

3.4. Battery Capacity Degradation after External Short Circuit

After experiencing external short circuit, side reactions occur inside the lithium-ion battery and generate side-reaction products. The structure of the battery materials is damaged to a certain extent, resulting in capacity degradation and increased impedance. This affects the service life of the battery. In the above experiments, different liquid cooling parameters affected the external short-circuit thermal behavior of the battery. To analyze the influence of external short circuit on battery life, the battery capacity and impedance were measured in this study, and the incremental capacity (IC) curve was obtained. Based on incremental capacity analysis (ICA), the aging mechanism of the battery was further investigated.

3.4.1. Capacity Changes before and after External Short Circuit under Different Experimental Conditions

The capacity degradation of lithium-ion batteries after external short circuit is shown in Table 4. As can be seen from Table 4, the capacity degradation of the battery after external short circuit was relatively severe, showing the highest capacity degradation among all experiments. After liquid cooling thermal management was applied, the capacity degradation of the battery after external short circuit was suppressed. The mechanisms of battery capacity degradation include loss of lithium inventory (LLI) and loss of active materials (LAM) in the positive and negative electrodes [19]. Among them, LLI is mainly caused by lithium plating and the growth of SEI and CEI, while LAM is caused by structural damage to the positive and negative active materials, particle cracking, graphite exfoliation, and reduction of active surface area.

During the external short-circuit process, lithium ions are rapidly extracted from the negative electrode and inserted into the positive electrode, which damages the SEI and CEI on the surfaces of the negative and positive electrodes. After the SEI and CEI are damaged, the electrolyte contacts with the positive and negative active materials, generating new CEI and SEI. The increase in battery temperature accelerates this process. In addition, the rapid insertion and extraction of lithium ions generate significant stress, leading to particle cracking of the positive and negative active materials and damage to the crystal structure of the materials. External short circuit also causes over-discharge, which further induces current collector corrosion and other side reactions. Liquid cooling thermal management reduces the battery temperature and suppresses the exothermic side reactions inside the battery, thereby suppressing capacity degradation.

Table 4. Capacity variation before and after external short circuit.

Experimental Condition	Before (Ah)	After (Ah)	Capacity Loss (%)
ESC	45.682	43.036	5.79
ESC-5 °C-1.5 L/min	46.252	45.581	1.45
ESC-10 °C-1.5 L/min	46.503	45.66	1.81
ESC-15 °C-1.5 L/min	43.049	42.132	2.13
ESC-5 °C-1 L/min	45.522	44.604	2.02
ESC-5 °C-0.5 L/min	43.785	42.755	2.35

Incremental capacity analysis is a commonly used method for analyzing the aging mechanism of lithium-ion batteries. The intensity and position of the peaks in the IC curve reflect the phase transition of battery electrodes and the changes in internal redox reactions. As shown in Figure 7, the IC curve of the battery before external short circuit has two peaks. The first peak mainly represents the insertion and extraction of lithium ions in the negative electrode, while the second peak mainly represents the phase transition of the positive electrode [20].

As shown in Figure 7a, after external short circuit, peak (1) in the IC curve disappeared, a new peak appeared, the IC curve even decreased to negative values, and peak (2) shifted to the right and decreased. This indicates the formation of SEI on the negative electrode and the loss of active lithium ions. The appearance of the new peak indicates that the crystal structure of the positive electrode was damaged and a new phase transition occurred. In addition, the rightward shift of peak (2) also indicates the loss of active lithium ions and active materials.

Under the 5 °C-1.5 L/min condition, peak (1) shifted toward a higher voltage and its peak value increased, while peak (2) also shifted to the right but its peak value decreased, indicating the loss of active lithium ions and active materials. In addition, two small peaks appeared in the IC curve, indicating changes in the crystal structure of the positive electrode material and the occurrence of new phase transitions. However, compared with the external short-circuit condition, the peak value of the new peak was relatively low.

As the coolant temperature increased, the battery capacity degradation under liquid cooling thermal management became more severe. As shown in Figure 7b–d, new peaks appeared in all batteries, peak (1) increased and shifted to the right, and peak (2) decreased and shifted to the right. With the increase in coolant temperature, peak (2) decreased more significantly, while the new peak value was higher under the 10 °C-1.5 L/min condition. External short circuit induces high-rate discharge, during which lithium ions are rapidly inserted into the positive electrode, causing greater damage to the crystal structure of the positive electrode and leading to more severe degradation of the positive electrode material. Battery capacity degradation can be comprehensively characterized by peak (1), peak (2), and the new peak. As shown in Figure 7e,f, with the decrease in coolant flow rate, the peak variations were similar, although the degree of peak change was different.

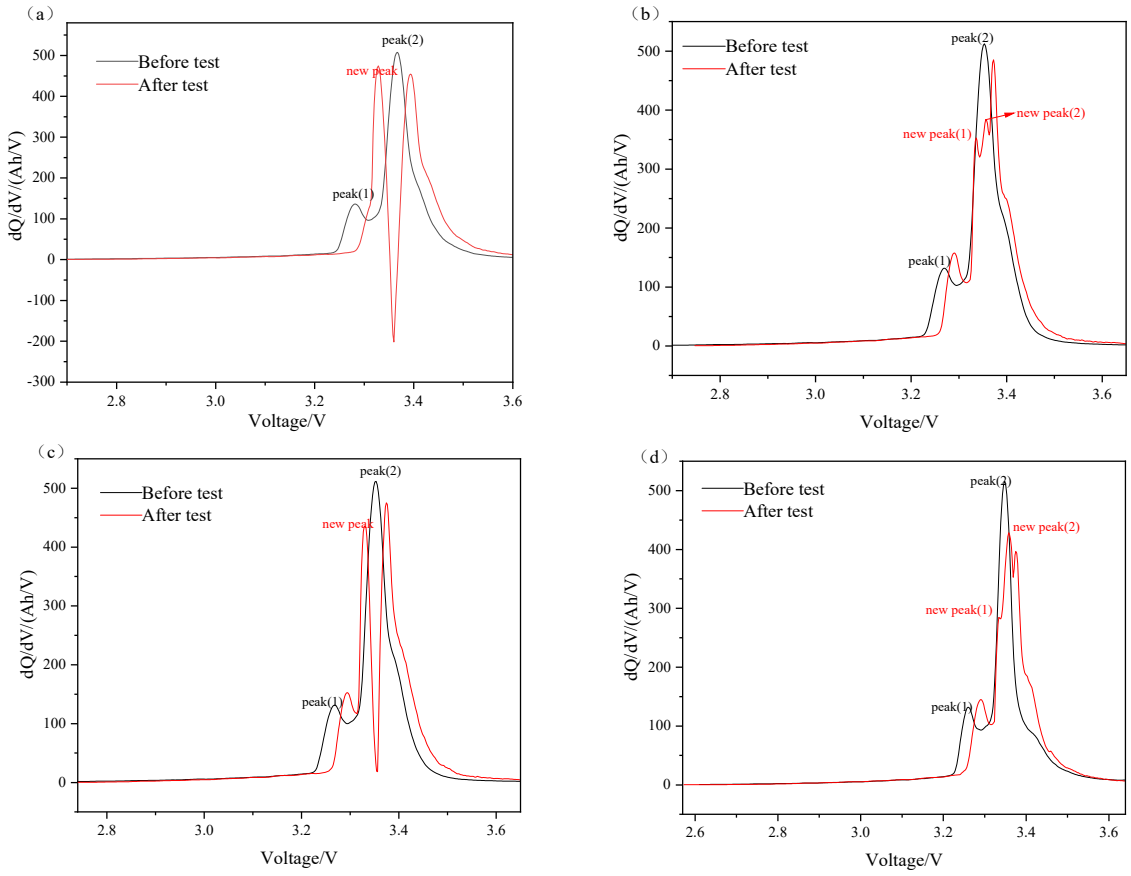

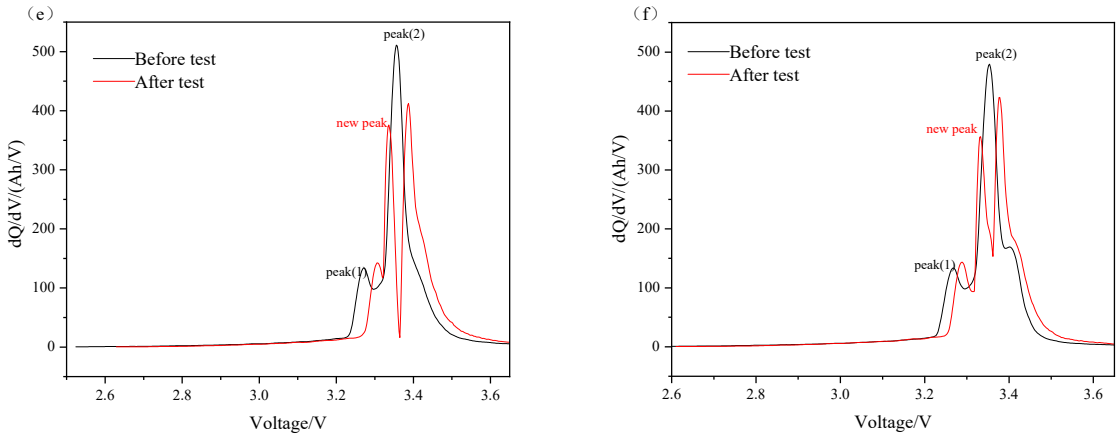

Figure 7. IC curves of batteries before and after external short circuit under different experimental conditions. (**a**) ESC test, (**b**) 5 °C-1.5 L/min, (**c**) 10 °C-1.5 L/min, (**d**) 15 °C-1.5 L/min, (**e**) 5 °C-1 L/min, (**f**) 5 °C-0.5 L/min.

3.4.2. Changes in Battery Impedance Under Different Experimental Conditions

After the external short circuit, the total resistance R_{tot}, ohmic resistance R_{Ω}, and polarization resistance R_p of all batteries are shown in Figure 8. The increase in battery impedance is attributed to electrode material degradation and internal side reactions in the battery [27]. As shown in Figure 8a, the impedance of the battery after external short circuit without liquid cooling was higher than that of all batteries after external short circuit under liquid cooling conditions. This indicates that after the external short circuit test, the internal structure of the battery was more severely damaged than in the other experiments, more decomposition products were generated on the surfaces of the positive and negative electrodes, and the internal resistance of the battery increased.

For the liquid cooling experiments, the battery internal resistance was the lowest under the 5 °C-1.5 L/min liquid cooling condition. With the increase in coolant temperature and the decrease in flow rate, the battery impedance increased. Compared with reducing the coolant temperature, increasing the coolant flow rate was more effective in reducing battery impedance. This is similar to effect of thermal management on the maximum temperature and capacity degradation of the battery after external short circuit.

Figure 8b shows the ohmic impedance of the battery. It can be found that when the liquid cooling flow rate remained unchanged, the ohmic impedance of the battery increased with increasing temperature. However, when the liquid cooling temperature remained unchanged and the flow rate decreased, the ohmic impedance of the battery instead decreased.

Figure 8c shows the polarization impedance of the battery. The polarization impedance of lithium-ion batteries is the impedance increased by internal electrochemical reactions in the battery. It can be found that the battery polarization impedance was the highest in the ESC experiment, indicating that the electrochemical reactions inside the battery were more intense during external short circuit. In the liquid-cooled external short-circuit experiments, the polarization impedance of the battery was relatively stable. As mentioned above, the introduction of liquid cooling can suppress the internal lithium-ion migration rate and electrochemical reactions during the external short-circuit process.

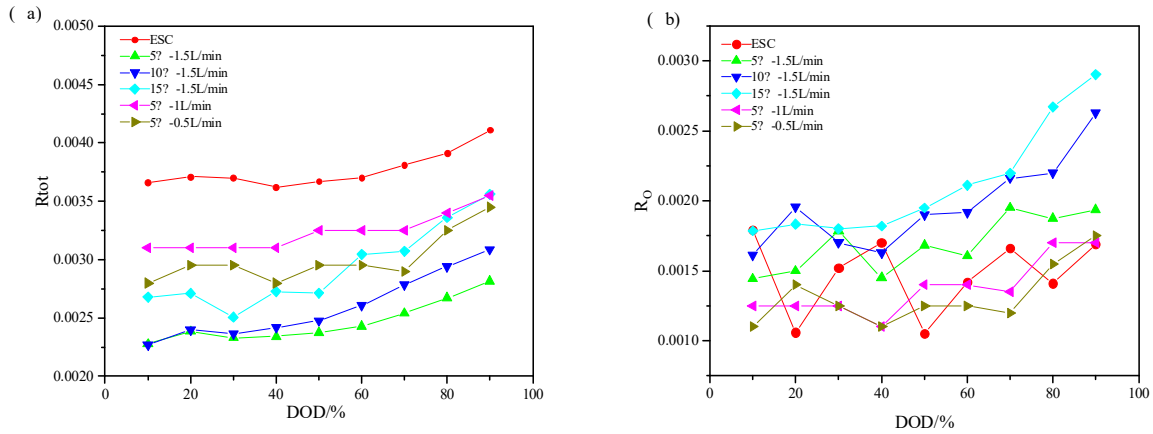

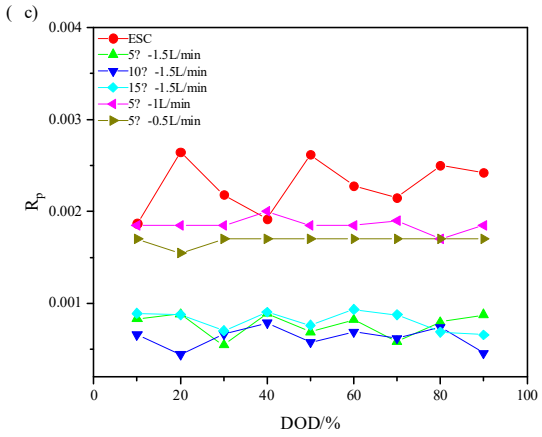

Figure 8. Internal resistance variation of batteries after external short circuit under different experimental conditions. (**a**) total resistance; (**b**) ohmic resistance; (**c**) polarization resistance.

The capacity degradation and impedance growth after external short circuit are closely associated with the same thermal electrochemical degradation processes. During the initial stage of external short circuit, the high discharge current generates substantial Joule heat, resulting in a rapid increase in battery temperature. The elevated temperature accelerates electrolyte decomposition and interfacial side reactions. Meanwhile, the rapid extraction and insertion of lithium ions damage the SEI and CEI layers and induce mechanical stress within the electrode particles. During the subsequent over-discharge stage, SEI decomposition, electrode structural damage, current-collector corrosion, and the formation of additional side-reaction products become more pronounced.

These changes cause loss of lithium inventory and loss of active material, resulting in a decrease in the available discharge capacity. The changes in the IC curves, including peak-value reduction, peak-position shifts, and the appearance of new peaks, indicate degradation of the electrode materials, consumption of active lithium, and changes in the electrode reaction processes. At the same time, the reformation and thickening of interfacial films, accumulation of side-reaction products, and deterioration of the electrode structure hinder electron conduction, lithium-ion transport, and charge-transfer reactions, thereby increasing the ohmic and polarization resistances. The increased impedance further intensifies battery polarization and reduces charge-discharge efficiency and usable capacity. Therefore, capacity degradation and impedance growth are not independent phenomena but are jointly caused by temperature rise, internal side reactions, interfacial film changes, and electrode structural damage.

As shown in Table 4, all batteries exhibited different degrees of capacity loss after external short circuit. Without liquid cooling, the battery experienced the most severe heat accumulation, and its capacity loss reached 5.79%, accompanied by the most pronounced IC curve changes and the highest post-test impedance. Under liquid-cooling conditions, the capacity loss decreased to 1.45–2.35%, while both the IC curve variation and impedance growth were alleviated. These results demonstrate that liquid cooling reduces irreversible electrochemical degradation by limiting battery temperature rise, suppressing internal side reactions, and alleviating damage to the electrode materials and interfacial films, thereby contributing to longer battery service life and improved post-fault safety.

4. Conclusions

Externals short circuit of 50 Ah prismatic $LiFePO_4$ battery and the influence of liquid thermal management system on external short circuit were studied in this work. The results of maximum temperature, capacity fading and resistance increase after different tests are compared to each other. The method to suppress the thermal hazard and capacity degradation after external short circuit can be obtained. The main conclusions are as follows:

(1) The external short-circuit process can be divided into five stages: rest, short-circuit initiation, current plateau, over-discharge heating, and cooling stabilization. Joule heat dominates the early and current-plateau stages, whereas side-reaction heat becomes more important during over-discharge and causes the battery temperature to reach its maximum value.

(2) Liquid cooling effectively suppresses battery temperature rise, heat accumulation, and internal side reactions. Without liquid cooling, side-reaction heat contributes more to the total heat generation compared to other conditions. At a constant coolant flow rate, increasing the coolant temperature weakens heat removal and increases the side-reaction heat contribution. At 5 °C, reducing the flow rate from 1.5 L/min to 0.5 L/min generally increases the contribution of side-reaction heat to total heat generation.

(3) External short circuit causes irreversible electrochemical degradation. The capacity loss reaches 5.79% without liquid cooling but decreases to 1.45–2.35% under liquid-cooling conditions. Incremental capacity and impedance analyses indicate active-lithium loss, electrode structural degradation, interfacial film changes, and impedance growth. Liquid cooling alleviates these degradation processes by limiting the battery temperature rise and suppressing side reactions.

Overall, liquid cooling not only reduces the immediate thermal hazard of external short circuit but also mitigates post-fault capacity loss and impedance deterioration.

Author Contributions

C.E: writing—original draft preparation, writing—reviewing and editing. X.J.: data curation. H.Z.: data curation. J.L.: investigation, validation. J.L.: conceptualization, methodology, supervision, reviewing and editing. All authors have read and agreed to the published version of the manuscript.

Funding

The authors are grateful for the support given by National Key R&D Program of China (2023YFC3009900), Natural Science Foundation of Jiangsu Province (BK20240543), National Natural Science Foundation of China (52272396,52474233).

Institutional Review Board Statement

Not applicable.

Informed Consent Statement

Not applicable.

Data Availability Statement

The data supporting the findings of this study are available upon request.

Conflicts of Interest

The authors declare no conflict of interest.

Use of AI and AI-Assisted Technologies

No AI tools were utilized for this paper.

References

1. Zhang, X.; Li, Z.; Luo, L.; et al. A review on thermal management of lithium-ion batteries for electric vehicles. *Energy* **2022**, *238*, 121652.
2. Harasis, S.; Khan, I.; Massoud, A. The impact of high ambient temperatures on lithium-ion batteries in electric vehicles: An in-depth review of thermal performance and chemistry-specific response. *Renew. Sustain. Energy Rev.* **2026**, *229*, 116623.
3. Yin, S.; Liu, J.; Cong, B. Review of thermal runaway monitoring, warning and protection technologies for lithium-ion batteries. *Processes* **2023**, *11*, 2345.
4. Shahid, S.; Agelin-Chaab, M. A review of thermal runaway prevention and mitigation strategies for lithium-ion batteries. *Energy Convers. Manag. X* **2022**, *16*, 100310.
5. Belgibayeva, A.; Rakhmetova, A.; Rakhatkyzy, M.; et al. Lithium-ion batteries for low-temperature applications: Limiting factors and solutions. *J. Power Sources* **2023**, *557*, 232550.
6. Piao, N.; Gao, X.; Yang, H.; et al. Challenges and development of lithium-ion batteries for low temperature environments. *Etransportation* **2022**, *11*, 100145.
7. Chowdhury, S.; Barrera, A.; Marinova, M.; et al. Impact of external short circuit on lithium-ion batteries: A post-mortem case study. *J. Mater. Chem. A* **2025**, *13*, 18600–18609.
8. Guo, D.; E, C.; Lu, Y.; et al. External short circuit of lithium-ion battery after low temperature aging. *Energy Technol.* **2026**, *14*, e202502074.
9. Chen, Z.; Xiong, R.; Lu, J.; et al. Temperature rise prediction of lithium-ion battery suffering external short circuit for all-climate electric vehicles application. *Appl. Energy* **2018**, *213*, 375–383.

10. Zhao, R.; Liu, J.; Gu, J. Simulation and experimental study on lithium ion battery short circuit. *Appl. Energy* **2016**, *173*, 29–39.
11. Liu, J.L.; Liu, J.L.; Jin, X.M.; et al. Influence of multi factors on external short circuit of lithium-ion battery. *Process Saf. Environ. Prot.* **2025**, *199*, 107279.
12. Yu, Z.X.; Chen, C.; Zhao, P.F.; et al. Thermal runaway-induced short-circuit arc in highly integrated lithium-ion battery systems: Mechanisms, thresholds, and mitigation strategies. *Commun. Eng.* **2026**, *5*, 101.
13. An, Z.; Zhao, Y.; Du, X.; et al. Experimental research on thermal-electrical behavior and mechanism during external short circuit for $LiFePO_4$ Li-ion battery. *Appl. Energy* **2023**, *332*, 120519.
14. Yang, R.; Xiong, R.; Ma, S.; et al. Characterization of external short circuit faults in electric vehicle Li-ion battery packs and prediction using artificial neural networks. *Appl. Energy* **2020**, *260*, 114253.
15. Zhao, Y.; Zhang, T.; Wang, C.; et al. Analysis and optimization of thermal management system for cylindrical power battery based on distributed liquid cooling plates. *Sci. China Technol. Sci.* **2024**, *67*, 3695–3706.
16. Hu, H.S.; Xu, J.X.; Li, J.Y.; et al. Immersion coupled direct cooling with non-uniform cooling pipes for efficient lithium-ion battery thermal management. *J. Energy Storage* **2025**, *116*, 116010.
17. Wu, C.; Sun, Y.; Tang, H.; et al. A review on the liquid cooling thermal management system of lithium-ion batteries. *Appl. Energy* **2024**, *375*, 124173.
18. Lai, Y.; Wu, W.; Chen, K.; et al. A compact and lightweight liquid-cooled thermal management solution for cylindrical lithium-ion power battery pack. *Int. J. Heat Mass Transfer* **2019**, *144*, 118581.
19. Li, H.X.; Chen, L.; Zuo, H.Y.; et al. Performance enhancement of a battery thermal management system using novel liquid cold plates with micro-channel featuring pin fins. *Energy* **2024**, *301*, 131731.
20. Wang, Z.X.; Zou, Z.W.; Zhou, Y.; et al. Performance comparison of battery cold plates designed using topology optimization across laminar and turbulent flow regime. *Int. J. Heat Mass Transfer* **2025**, *238*, 126450.
21. Zhang, L.; Cheng, X.; Ma, Y.; et al. Effect of short-time external short circuiting on the capacity fading mechanism during long-term cycling of $LiCoO_2$/mesocarbon microbeads battery. *J. Power Sources* **2016**, *318*, 154–162.
22. An, Z.; Wang, L.; Du, X.; et al. The influence of external short-circuit durations on the performance and thermal runaway risk of lithium-ion battery under critical C-rate conditions. *J. Energy Storage* **2025**, *135*, 118372.
23. Liu, J.L.; Zhang, Y.; Bai, J.L.; et al. Influence of lithium plating on lithium-ion battery aging at high temperature. *Electrochim. Acta* **2023**, *454*, 142362.
24. Gotz, J.D.; Galvão, J.R.; Viana, E.R.; et al. A random forest mechanism to identify the initial conditions of external short circuits in 18650 lithium-ion batteries. *Ionics* **2025**, *31*, 3323–3339.
25. Morali, U. Influence of convective heat transfer coefficients on thermal behaviour of a lithium-ion cell: A numerical study. *Turk. J. Chem.* **2024**, *48*, 128–136.
26. Kovács, G.; Kocsis Szürke, S.; Fischer, S. Investigation of convective and radiative heat transfer of 21,700 lithium-ion battery cells. *Batteries* **2025**, *11*, 246.
27. Vetter, J.; Novák, P.; Wagner, M.R.; et al. Ageing mechanisms in lithium-ion batteries. *J. Power Sources* **2005**, *147*, 269–281.